Contribution of Backbone Dynamics to Entropy Changes Occurring on Oxidation of Cytochrome b_5. Can Redox Linked Changes in Hydrogen Bond Networks Modulate Reduction Potentials?

Bindi Dangi,[†] Jeffrey I. Blankman,[‡] Cary J. Miller,*[,‡,§] Brian F. Volkman,[||] and R. D. Guiles*[,†,⊥]

Department of Pharmaceutical Sciences, School of Pharmacy, University of Maryland, 20 North Pine Street, Baltimore, Maryland 21201, The Medical Biotechnology Center, an institute of the Maryland Biotechnology Institutes, 725 W Lombard Street, Baltimore, Maryland 21201, Department of Chemistry and Biochemistry, University of Maryland, College Park, Maryland 20742, and Nuclear Magnetic Resonance Facility at Madison, University of Wisconsin, Madison, Wisconsin 53706

Received: February 9, 1998; In Final Form: April 13, 1998

Changes in backbone dynamics occurring upon oxidation of rat cytochrome b_5 have been examined through model free analyses of ^{15}N-relaxation rates of both oxidation states of the protein. Based on the observed changes, an upper bound for the contribution of backbone dynamics to the entropy change associated with oxidation has been calculated. The magnitude of this backbone contribution, 70 ± 7 J/K·mol, is strikingly similar to the total entropy change associated with oxidation of the protein determined through an analysis of the temperature dependence of the reduction potential. Origins of the differences in dynamic behavior of the oxidized and reduced proteins can be attributed to redox linked changes in hydrogen bond strengths based on large-scale differences in amide proton exchange rates observed between the oxidation states. Based on these observations the magnitude and possible significance of entropic contributions to the electromotive force are discussed. Analysis of the ^{15}N-relaxation rates included modeling of anisotropic diffusional behavior which was expected based on the distinct physical asymmetry of the protein. An axially symmetric diffusion tensor model was found to fit the rotational reorientational properties of the protein in both oxidation states. The contribution of paramagnetic relaxation to the ^{15}N-relaxation rates of the oxidized protein was calculated based on a set of modified Solomon−Bloembergen equations. The determination of the electronic correlation time of the paramagnetic center was based on fits to the proton relaxation rate enhancements of protons in close proximity to the paramagnetic center. Analyses of the dynamic properties of the oxidized cytochrome b_5 were based on multiple field (i.e., 500 and 750 MHz) NMR measurements of ^{15}N T_1 and T_2 relaxation times.

Cytochromes are a class of ubiquitous electron-transfer proteins involved in important biological processes such as respiration, photosynthesis, and xenobiotic degradation.[1] Reduction potentials of these electron carriers span an enormous range (i.e., ∼600 mV). *b*-type cytochromes are a subclass of this type of electroactive protein. Even within this subclass of the cytochromes, reduction potentials span a range of nearly 400 mV.[2] In some instances a conformational change in a *b*-type cytochrome can induce a change in the reduction potential which spans nearly the entire observed range.[3] Cytochrome b_5 has become a model system for the study of protein heme interactions that control *b*-type cytochrome reduction potentials largely because it was the first protein in this class to be structurally characterized.[4]

Theoretical[5,6] and experimental approaches[7−10] examining factors that control cytochrome reduction potentials have focused on structural changes which shift the energy levels of the heme system due to changes in the charge distribution surrounding the heme,[6−8] changes in the orientation of the axial imidazole ligands to the iron,[9,10] or changes in the strength of hydrogen bonds to these axial imidazoles.[11] Here we examine the effects of entropy changes on the reduction potential and discuss the possible origins of these entropy changes.

We have taken two experimental approaches in attempting to understand the entropic contributions to the electromotive driving force: the temperature dependence of the reduction potential explored using surface modified electrodes[10,12,13] and NMR methods in the characterization of backbone dynamics.[14,15] In addition, to gain some insight into the origin of observed changes in backbone dynamics occurring upon oxidation, changes in amide deuterium exchange rates were examined.[16] Significant differences in generalized order parameters obtained from the ^{15}N-relaxation analyses are then used in an estimate of an upper bound for the contribution of backbone dynamics to the observed entropy change.[17] Finally the magnitude of the contribution of the entropic term to the electromotive driving force is discussed relative to the magnitude of energetic factors previously described.

[†] Department of Pharmaceutical Sciences, School of Pharmacy, University of Maryland.
[‡] Department of Chemistry and Biochemistry, University of Maryland.
[§] Current address: i-Stat Corporation, Kanata, ON, Canada K2L 1T9.
[||] University of Wisconsin, Madison.
[⊥] The Medical Biotechnology Center.

S1089-5647(98)01050-5 CCC: $15.00
Published on Web 05/22/1998

Experimental Details

Electrochemical Measurements. Electrochemical measurements were performed by using surface-modified electrodes consisting of gold surfaces modified by self-assembling monolayers composed of ω-hydroxyalkanethiols.[18] Details and advantages of these electrode systems in their application to heme protein electroreactivity have been described in detail previously.[10,12,13] Briefly, gold electrodes (0.13 cm^2 active surface area) were prepared by sputtering a chromium adhesion layer on to glass plates followed by a gold layer roughly 2000 Å thick. The ω-hydroxyalkanethiols were synthesized and purified as described previously.[18] Gold electrodes were rigorously cleaned by immersion in strong chromic acid, followed by aqueous HF, and finally rinsed with deionized water. Self-assembly of the monolayers occurs spontaneously when the gold electrodes are immersed in ethanolic solutions of the ω-hydroxyalkanethiols.

Electrochemical measurements were performed by using a three electrode system employing a platinum counter electrode and saturated calomel reference electrode in a jacketed conical cell with a volume of about 300 μL. Cyclic voltammograms were recorded with a Bioanalytical Systems BAS100B potentiostat and waveform generator. The temperature was maintained within 0.1 °C using a Fisher Scientific thermostat (Model 9101).

Reduction potentials were determined by taking the average of the inflections of anodic and cathodic waves determined by the maximum in the analytic derivative of the voltammetric currents recorded by using short ω-hydroxyalkane thiols (e.g., $HO(CH_2)_2SH$ or $HO(CH_2)_3SH$). By use of these short ω-hydroxyalkanethiols, maximum sensitivity is obtained in a diffusion-limited regime and the effects of electrode passivation due to adsorption of the protein onto a bare metallic electrode surface are minimized.

Reorganizational energies were determined with longer chain length ω-hydroxyalkanethiols (e.g., $HO(CH_2)_6SH$ to $HO(CH_2)_{14}SH$). Following corrections for residual diffusion-limited currents and for double layer effects,[19] the reorganizational energy is obtained by fitting the derivative of the votammetric current with respect to the applied potential to the Marcus theory equation.[18] Double-layer corrections were based on effective charges determined by measuring the ionic strength dependence of the current.[19]

Deuterium Exchange Experiments. Deuterium exchange rates of amide protons were measured by dissolving the rat cytochrome in D_2O solutions of 100 mM phosphate buffer pH 7.0 and recording heteronuclear correlation spectra at regular intervals (e.g., 10 min, 30 min, 1 h, 2 h, 4 h, 8 h, 16 h, and 32 h) by using the fast-HSQC sequence.[20] All NMR spectra were processed with NMRPipe.[21] Cross-peak intensties were determined by fitting cross-peaks to a Gaussian line shape and determining peak heights. Time constants for exchange were then determined by fitting the decay curves to a single two-parameter exponential. Uncertainties were determined through replicate experiments. For the reduced protein, a small quantity of solid sodium dithionite was added to the NMR sample immediately after dissolution in the D_2O buffer. An anaerobic atmosphere was maintained through the use of NMR tubes which were purged with nitrogen prior to sealing with a Teflon stopcock (Wilmad Glass, Co.). Deuterium exchange rates for the reduced protein have been reported previously.[15]

Changes in Backbone Dynamics Determined through the Analysis of ^{15}N-Relaxation Measurements of Both Oxidation States. The analysis of the backbone dynamics of rat ferrocytochrome b_5 have been described in detail previously.[15] The analysis included an anisotropic diffusional analysis[22,23] of the hydrodynamic properties of the protein due to the marked physical anisotropy of the protein indicated by the known crystal structure[4] and recent NMR solution structures of the reduced protein.[15,24] All $^{15}N-^{1}H$ correlation peaks for the backbone amides of both oxidized[25,26] and reduced rat cytochrome b_5[15,27] have been unambiguously assigned based on interpretation of a set of double and triple resonance experiments described previously.

A similar approach has been taken in the analysis of the oxidized protein; however, additional complications due to the paramagnetism of the oxidized protein had to be addressed. The analysis of the backbone dynamics assumes that the ^{15}N-relaxation rates are dominated by interproton dipolar couplings and ^{15}N-chemical shift anisotropy.[28] Therefore the magnitude of electron−nuclear relaxation effects has to be assessed. The effects of electron nuclear relaxation were assessed by fitting modified Solomon−Bloembergen equations (eqs 1 and 2) to the ^{1}H-relaxation rates observed in the oxidized protein. Equation 1 was derived by Bertini et al.[29] for the case of a protein in the slow tumbling regime where the electron correlation, τ_e, time is much faster (e.g., by at least 2 orders of magnitude) than the global protein correlation time, τ_c.

$$T_{1M}^{-1} = \frac{2}{15}\left(\frac{\mu_0}{4\pi}\right)^2\left[\frac{\gamma_I^2\mu_B^2 S(S+1)\tau_S}{r^6}\right]\left\{\left[\frac{1}{1+(\omega_S^{av})^2\tau_S^2}\right]\times\left[7\left(g+\frac{a}{2}\right)^2+5a^2+\frac{13}{3}\left|b\right|^2+\frac{7}{12}\left|c\right|^2\right]+\left[\frac{1}{1+\omega_I^2\tau_S^2}\right]\times\left[3\left(g+\frac{a}{2}\right)^2+4\left|b\right|^2+\frac{|c|^2}{4}\right]\right\} \quad (1)$$

$$T_{2M}^{-1} = \frac{2}{15}\left(\frac{\mu_0}{4\pi}\right)^2\left[\frac{\gamma_I^2\mu_B^2 S(S+1)\tau_S}{r^6}\right]\left\{\left[\frac{1}{1+(\omega_S^{av})^2\tau_S^2}\right]\times\left[\frac{13}{2}\left(g+\frac{a}{2}\right)^2+\frac{5}{2}a^2+\frac{37}{6}\left|b\right|^2+\frac{13}{24}\left|c\right|^2\right]+\left[\frac{1}{1+\omega_I^2\tau_S^2}\right]\times\left[\frac{3}{2}\left(g+\frac{a}{2}\right)^2+2\left|b\right|^2+\frac{|c|^2}{8}\right]+2\left(g+\frac{a}{2}\right)^2+\frac{5}{2}a^2+\frac{|b|^2}{2}+\frac{|c|^2}{6}\right\} \quad (2)$$

where $g = {}^1/_3(g_{xx}+g_{yy}+g_{zz})$, $g' = g_{zz}-g$, $\eta = (g_{yy}-g_{xx})/g'$, $\omega_S^{av} = \omega_S(g/ge)$, and the angular dependencies relative to the magnetic axes are given by

$$a = -\frac{g'}{2}\left[1-3\cos^2\theta+\eta\cos 2\phi\sin^2\theta\right]$$

$$b^2 = \left(\frac{g'}{2}\right)^2\left\{\left[\frac{3}{2}\sin 2\theta+\frac{\eta}{2}\sin 2\theta\cos 2\phi\right]^2+\left[\eta\sin 2\phi\sin\theta\right]^2\right\}$$

$$c^2 = \left(\frac{g'}{2}\right)^2\{[1 - 3\sin^2\theta + \eta\cos 2\phi\,(1 + \cos^2\theta)]^2 + [2\eta\sin 2\phi\cos\theta]^2\}$$

Using an approach analogous to that used by Bertini et al.[29](e.g., the assumption of a single correlation time, designated τ_S here, which is defined by $1/\tau_S = 1/\tau_e + 1/\tau_c$) in deriving eq 1 from the equations previously developed by Vasavada and Rao,[30] we have derived an expression for T_2. More general algorithms describing paramagnetic relaxation of nuclear spins encompassing the approximations used in the equations shown here have recently been developed.[31] Because the electron nuclear relaxation rates depend on the square of the nuclear magnetogyric ratio, the ^{1}H relaxation rates should be dominated by the electron−nuclear dipolar interaction for protons sufficiently close to the paramagnetic center. Nitrogen-15 paramagnetic relaxation rates which are roughly 100-fold lower than proton relaxation rates can then be calculated given the value of the electron correlation time determined from fitting the proton relaxation rates and the known structure of the protein. Note, the fit to eqs 1 and 2 were one parameter fits to the observed rate enhancements relative to rates observed for the reduced protein, in that the magnetic axes and the magnitude of magnetic anisotropy have been determined from fits to the pseudocontact effects observed in cytochrome b_5[25] and from EPR spectra recorded for the protein.[10] Proton T_1 relaxation times in oxidized and reduced proteins were measured using heteronuclear single quantum correlation experiments described by Kay et al.[32] Rate enhancements due to the paramagnetism were fit to eq 1. The contributions to the ^{15}N R_1 and R_2 relaxation rates were determined from eqs 1 and 2 and the known structure of the protein.[4]

Based on the calculated electron nuclear relaxation rates for ^{15}N R_1 and R_2 values, small corrections (e.g., less than 10% of the observed rates) were applied for a small number of residues close to the heme iron. At the present time, it is not clear what the effect this enhanced electron nuclear relaxation is going to have on the NOE amplitude in that both ^{1}H and ^{15}N relaxation rates may be important in determining this amplitude. Therefore we did not use NOE amplitudes in the modeling of the protein's spectral density function. Instead, we measured T_1 and T_2 relaxation times at 500 and 750 MHz and fit the observed rates using the model free formalism developed by Lipari and Szabo.[33,34] Analysis of the ^{15}N-relaxation parameters were performed by using the ModelFree 3.1 suite of programs developed and distributed by Palmer et al. (For reviews of the development and application of these programs see Palmer et al.[14,28])

The model free approach uses the relationship between ^{15}N-relaxation parameters and five spectral density function amplitudes as shown in eq 3.[35] Because, in general, fewer than five experimentally determined rate constants are measured, the spectral density function is modeled as a sum of Lorenztian terms[33,34] (eq 3).

$$R_1 = 1/T_1 = d^2[J(\omega_H - \omega_N) + 3J(\omega_N) + 6J(\omega_H + \omega_N)] + c^2J(\omega_N)$$

$$R_2 = 1/T_2 = 0.5d^2[4J(0) + J(\omega_H - \omega_N) + 3J(\omega_N) + 6J(\omega_H) + 6J(\omega_H + \omega_N)] + (1/6)c^2[J(\omega_N) + 4J(0)]$$

$$\mathrm{NOE} = 1 + (\gamma_H/\gamma_N)d^2[6J(\omega_H + \omega_N) - J(\omega_H - \omega_N)]T_1 \quad (3)$$

where $d^2 = 0.1[\gamma_H\gamma_N h/(2\pi\langle r^3_{HN}\rangle)]^2$ and $c^2 = (2/15)[\omega_N^2(\sigma_{||} - \sigma_\perp)$, $J(\omega)$ is the spectral density function, γ_i is the gyromagnetic ratio of nucleus i, h is Planck's constant, r_{HN} is the internuclear ^{1}H−^{15}N distance, assumed to be 1.02 Å, and $\sigma_{||} - \sigma_\perp$ is the difference between parallel and perpendicular components of the ^{15}N-chemical shift tensor.

For the isotropic case, spectral density funtions of the form shown in eq 4 are employed.[36]

$$J(\omega) = S^2\left[\frac{\tau_c}{1 + (\omega\tau_c)^2}\right] + (1 - S^2)\left[\frac{\tau'}{1 + (\omega\tau')^2}\right] \quad (4)$$

where $1/\tau' = 1/\tau_c + 1/\tau_f$, τ_c is the global correlation time of the protein, τ_f is a measure of short time scale motions of the amide vector relative to the global motion, and S is a generalized order parameter which is a measure of the amplitude of local amide vector motions on the fast time scale. The larger the S^2 value, the smaller the amplitude of angular freedom of movement.

For anisotropic molecular motions which can be modeled with an axially symmetric diffusion tensor, the spectral density function takes the following form:[37]

$$J(\omega) = S^2\left\{\frac{A_1\omega\tau_1}{1 + (\omega\tau_1)^2} + \frac{A_2\omega\tau_2}{1 + (\omega\tau_2)^2} + \frac{A_3\omega\tau_3}{1 + (\omega\tau_3)^2}\right\} + (1 - S^2)\left[\frac{\tau'}{1 + (\omega\tau')^2}\right] \quad (5)$$

where $A_1 = 0.75\sin^4\alpha$, $A_2 = 3\sin^2\alpha$, $A_3 = (1.5\cos^2\alpha - 0.5)^2$ $\tau_1 = (4D_{||} + 5D_\perp)^{-1}$, $\tau_2 = (D_\perp + 5D_{||})^{-1}$, $\tau_3 = (6\,D_\perp)^{-1}$, and α is the polar angle relative to the major axis of the diffusion tensor.

Finally, based on differences observed in the calculation of order parameters determined from fitting the ^{15}N-relaxation data, an upper bound to the contribution of backbone dynamics to the entropy change occurring upon oxidation of cytochrome b_5 can be calculated using an equation (eq 6) derived by Akke et al.[17]

$$\Delta S = k\sum_n \ln\left(\frac{1 - S_{n^2}^2}{1 - S_{n^1}^2}\right) \quad (6)$$

Where in this specific case the initial state (state 1) is the reduced state and the final state is the oxidized state (state 2) of cytochrome b_5. The summation index runs over all residues numbers containing ^{15}N−^{1}H amide vectors for which order parameters are known in both oxidation states.

Materials

Nitrogen-15 labeled cytochrome b_5 was expressed and isolated as previously described.[26] The model porphyrin compound iron bis(pyridine)tetrakis(sulfophenyl)porphyrin was synthesized and characterized using a slight modification of a published procedure.[38,39] Horse-heart myoglobin samples were prepared for electrochemistry by using commerially available material (Sigma Chemical Co.) following purification using gel exclusion chromatography (Pharmacia S100 column chromatography) and ion exhange chromatography (Phamacia DEAE column chromatography) as described previously.[13,40]

Results

The temperature dependence of the reduction potentials of rat cytochrome b_5 myoglobin and the model heme compound,

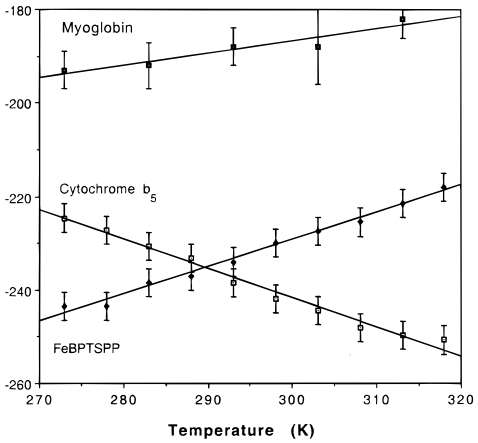

Figure 1. Temperature dependence of the reduction potentials of cytochrome b_5, iron bis(pyridine)tetrakis(sulfophenyl)porphyrin (FeBPTSPP), and myoglobin. Uncertainties are based on five replicate experiments.

TABLE 1: Thermodynamic, Transport, Charge State, and Electrochemical Properties of Rat Cytochrome b_5, Iron Bis(pyridine)Tetrakis(sulfophenyl)porphyrin, and Myoglobin

species	$E^{\circ\prime}$,[a] (V vs SCE)	D_o,[a] ($\times 10^7$ cm^2/s)	Z_{eff}	λ,[a] eV	ΔS_{ox},[b] J/K·mol
cytochrome b_5	−0.213	3.8 ± 0.8	−1.4	0.43 ± 0.02	60 ± 7
FeBPTSPP	−0.273	21 ± 6	−3.0	0.93 ± 0.08	-56 ± 7
myoglobin	−0.196	7.5 ± 0.8	0.6	0.76 ± 0.08	-25 ± 19

[a] Formal potentials, diffusion coefficients, and reorganizational energies were measured at 0.0 °C. Results presented here are reproduced from ref 13 for cytochrome b_5 and myoglobin and ref 39 for FeBPTSPP. Uncertainties are based on results from five replicate experiments. Uncertainties in the reduction potentials are ±3 mV. Accurate determinations of the diffusion coefficients and the effective charge are important for the corrections for residual diffusion currents and double layer effects in the calculation of the reorganizational energy.[13] [b] The entropy change observed on oxidation is derived from the temperature dependence of the reduction potential (see Figure 1) as described in the text. Statistical confidence in the entropy change for myoglobin is low due to greater uncertainties in the determination of the reduction potential at higher temperatures. Correlation coefficients for the fits to the data shown in Figure 1 are $r^2 = 0.984$, 0.990, and 0.899 for cytochrome b_5, FeBPTSPP, and myoglobin, respectively.

iron bis(pyridine)tetrakis(sulfophenyl)porphyrin, are shown in Figure 1. Excellent linearity is observed over the range of temperatures investigated for the model compound and cytochrome b_5. The behavior of myoglobin is less well defined although a reproducible trend was observed. The reduction potentials can be converted to free energies by multiplying by minus one times Faraday's constant given the fact that the redox couples involve one electron transfers. From the slope of the temperature versus free energy line one can obtain the entropy change upon oxidation. Table 1 contains electrochemical parameters determined for cytochrome b_5, the model heme compound, and myoglobin.

Striking differences are observed in the behavior of the model compound and cytochrome b_5. As we have previously described, the primary difference between the reorganizational energies of cytochrome b_5 and the heme model compound is the outer sphere contribution to the reorganizational energy.[39] The solvent reorganizational energy term is the energy cost in charging a high dielectric medium such as water;[41] however, a molecular interpretation would involve increased electrostatic interaction of the solvent with the more positive center in the oxidized state, a concept similar to solvent electrostriction.[42] Thus, associated with this energetic effect is an intrinsic entropic effect on outer sphere solvent molecules which we believe is the dominant origin of the negative entropy change occurring on oxidation of the model compound.

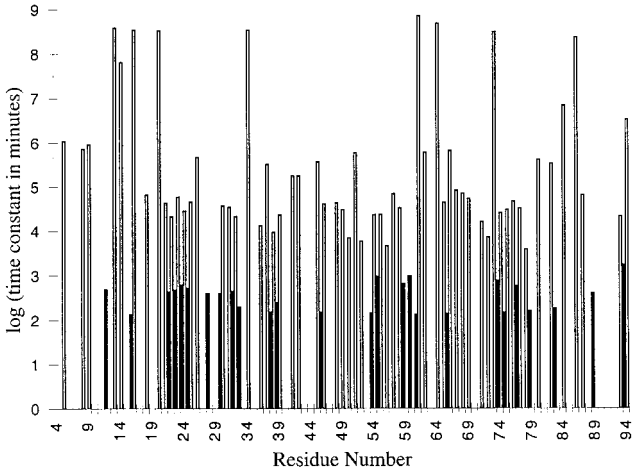

Figure 2. Deuterium exchange time constants observed for ferro- and ferricytochrome b_5 plotted as a function of residue number. Black bars represent the exchange times of the oxidized cytochrome. White outlined bars represent the reduced cytochrome. The absence of a bar is due to either a rate which was faster than the first time point in the measurements (e.g., 10 min) or corresponds to a proline. Because of the enormous range of values observed the time constants were plotted on a log scale.

The hydrophobic environment of the heme binding domain of the cytochrome reduces this outer sphere reorganizational energy term to a negligible contribution. However, the entropy change in the cytochrome is a large positive term, almost equal in magnitude to the negative entropy change observed in the model. Experiments evaluating ^{15}N-relaxation properties and amide deuterium exchange rates in oxidized and reduced states described below were performed to evaluate the contribution of redox linked changes in protein backbone dynamics to the observed entropy change.

Deuterium Exchange. Figure 2 contains rates of exchange observed for both the reduced and the oxidized cytochrome b_5. Dramatic differences in the rates of exchange are observed. A significant fraction of amide exchange rates have increase by several orders of magnitude. In general, amide proton exchange rates fall into two categories; rates determined only by the pH of the solution and the pK_a of the amide and rates limited by the rate of intramolecular hydrogen bond opening.[43] In the latter case the rate of hydrogen bond opening can depend on very local effects or global or subglobal unfolding of the protein. Thus, the rates are limited by thermodynamic barriers between partially unfolded and native states of a protein. As a result, the analysis of the contributions of individual amide exchange rates to the total thermodynamic stability of the protein can be quite complex. However, the changes observed here are strongly suggestive of large scale changes in the rigidity of the protein which occur on oxidation. Because it is also more difficult to quantitatively relate changes in amide exchange rates to entropy changes associated with some chemical process, changes in backbone dynamics were examined. The backbone dynamic analyses described below are more suited to evaluating contributions to the entropy change[17] observed upon oxidation.

Protein Dynamic Analyses. The analysis of the dynamic behavior of rat ferrocytochrome b_5 has been reported previously.[15] Results of that analysis are described here for comparative purposes, to understand the changes which occur upon oxidation. The analysis of the dynamics of the oxidized protein paralleled that of the reduced protein in that anisotropic

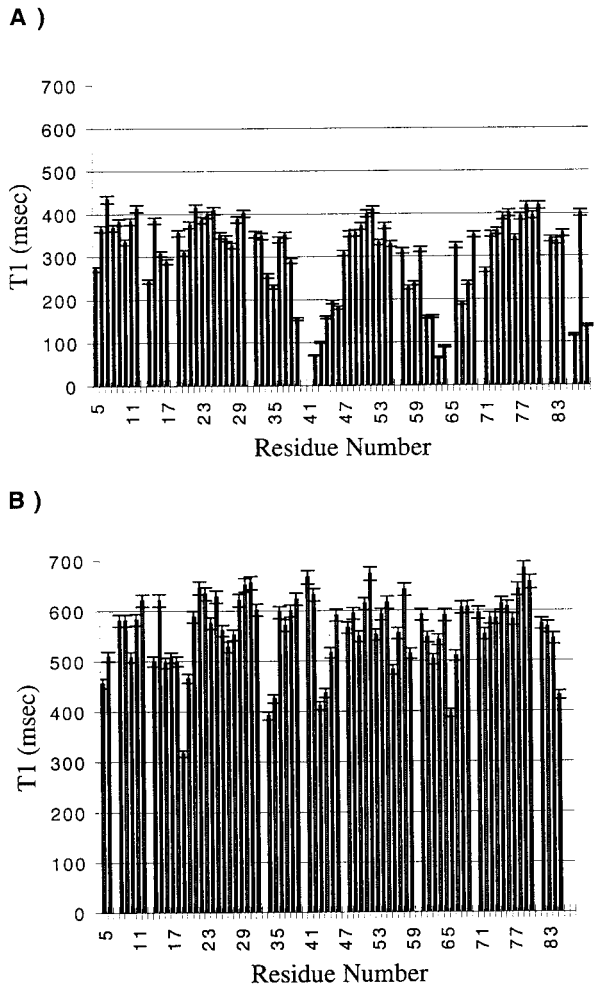

Figure 3. Proton T_1 relaxation times plotted as a function of residue number for both oxidized (A) and reduced (B) rat cytochrome b_5.

models[22] for the global reorientation properties were evaluated and model free analyses[36] of amide vector reorientation were used to extract values for the generalized order parameter. The primary difference in the analysis of the oxidized protein lies in the evaluation of the contribution of paramagnetic relaxation.

Proton relaxation times determined from fits to the decay of the proton magnitization observed in heteronuclear correlation experiments are shown in Figure 3. From a comparison of the proton T_1 relaxation times shown in Figure 3, it is clear that the paramagnetism of the oxidized protein enhances amide proton relaxation rates throughout the molecule, but the effect is most pronounced for residues in close proximity to the heme (e.g., most prominently in helices 3 and 5). Fits to eqs 1 and 2 only involve a single parameter, the electronic correlation time. This parameter also has limitations on the range of values of τ_e which are physically realistic (e.g., from 10^{-11} to 10^{-12} s).[44] Only the largest proton relaxation rates were fit to eq 1 in that these rates are dominated by electron nuclear relaxation by protons that are close to the heme center and the diamagnetic rate is being approximated by the rates measured for the reduced protein. This approximation is clearly valid when rates are at least doubled by the effect of paramagnetic relaxation, however, as is clear from the results of the comparative dynamics analysis, the reduced protein is significantly more rigid than the oxidized protein. However, these differences are only on the order of 15% in the relaxation rates observed in T_1 and T_2 and reflected in similar magnitude in the order parameter, S^2.

In addition it is important to point out that certain residues

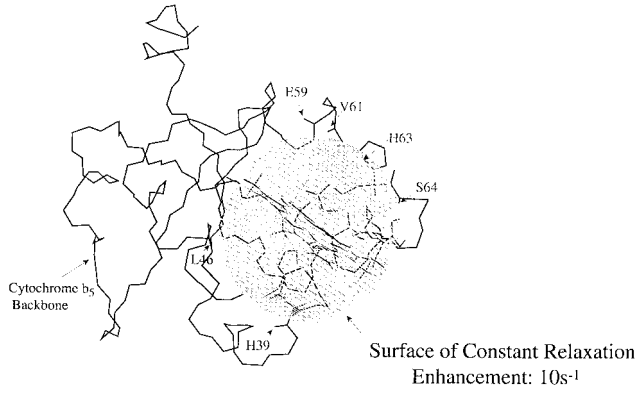

Figure 4. Calculated surface of constant R_1 relaxation enhancement mapped onto the backbone structure of cytochrome b_5. The structure of cytochrome b_5 shown is that of the oxidized bovine protein; however, recent solution structure determinations of the rat protein are nearly indistinguishable (e.g., rms overlays indicate mean square differences on the order of one angstrom).

TABLE 2: Observed and Calculated Relaxation Rate Enhancements for Those Amide Protons and Nitrogens Closest to the Fe Center

residue	obsd rate,[a] (s^{-1})	calcd rate[b], (s^{-1})	r(Fe−H)[c] (Å)	calcd ^{15}N R_1,[d] (s^{-1})	calcd ^{15}N R_2,[d] (s^{-1})
H63	13.60	13.48	6.75	0.14	0.17
S64	9.26	9.10	7.05	0.06	0.07
H39	4.88	4.93	7.97	0.07	0.08
V61	4.63	5.43	7.80	0.04	0.04
L46	3.85	4.50	7.89	0.04	0.05
E59	2.28	2.66	8.73	0.04	0.05

[a] The observed R_1 rate enhancement is the difference between the diamagnetic rate of the ferrocytochrome b_5 and the paramagnetic rat of ferricytochrome b_5. [b] The calculated rates are based on a one parameter fit to eq 1. From the fit to eq 1 a value of $(1.0 \pm 0.2) \times 10^{-11}$ s was obtained for the electron correlation time. The uncertainty in the electron correlation time was estimated based on the point at which the least-squares residual fit doubled on either side of the optimum value. [c] The iron−proton distances observed in the bovine crystal structure.[4] [d] Calculated values for nitrogen relaxation enhancements of R_1 and R_2 relaxation rates for the amide nitrogens of the residues indicated are calculated based eqs 1 and 2 and the value of τ_e obtained from the fit to the proton relaxation enhancements. Positions of the nitrogens in the magnetic axis system of the ferricytochromes g-tensor were determined from the bovine crystal structure. Note that even the largest paramagnetic contribution to the rate of ^{15}N relaxation is only on the order of 10% of the rate measured for that amide ^{15}N nucleus in that these values range from 1.2 to 2.0 s^{-1} for R_1 and from 4.3 to 8.3 s^{-1} for R_2 for the oxidized protein. Note the lowest rates correspond to residues in the N- and C-termini and in some flexible loops.

exhibited anomalous proton relaxation rates based on a fit to a single structural model. These residues (e.g., G42, E43, and E44) are in a region of the protein which exhibits the highest deuterium exchange rates (among the helices of the four helix bundle which forms the binding domain of the heme) and which previous molecular dynamics[45] and proton NMR experiments[46] have indicated that there is a degree of fluxionality which is not well modeled by a single static structure.

Figure 4 contains a plot of a surface of constant R_1 relaxation enhancement calculated using eq 1. The positions of amide protons used in fitting eq 1 to the value of the electronic correlation time are indicated in the figure. Table 2 contains observed and calculated rates for the protons with the largest rate of enhancement due to paramagnetic relaxation effects. It is clear from Figure 4 that the sixth power dependence of the electron nuclear relaxation dominates the rates with the magnitude of anisotropy characteristic of low spin hemes. Based

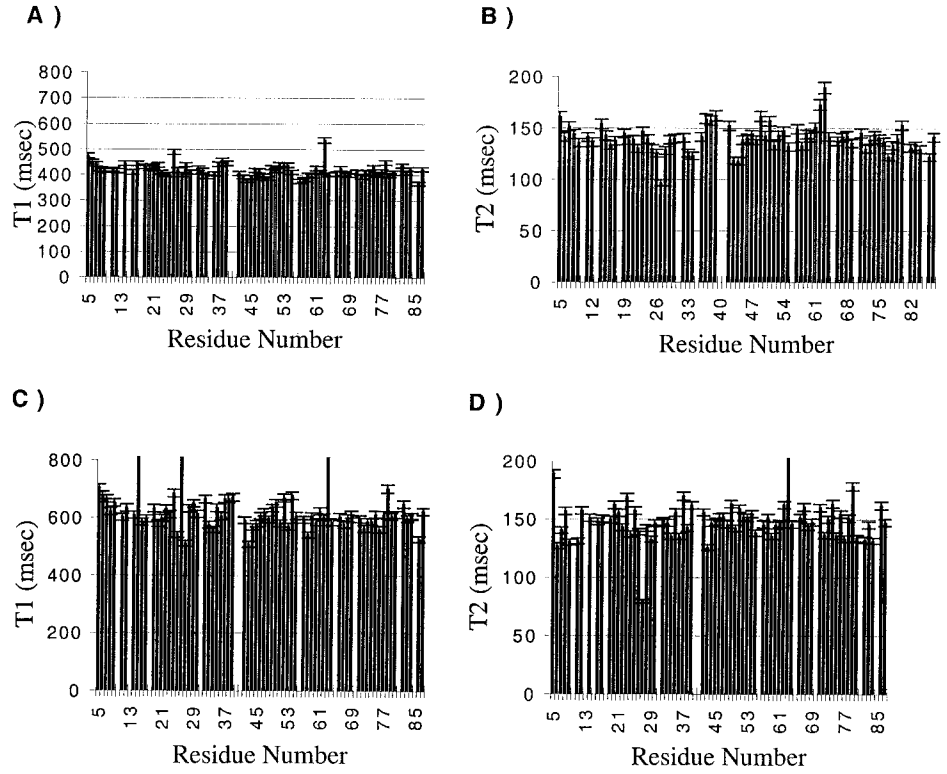

Figure 5. ^{15}N-relaxation rate constants observed for ferricytochrome b_5 at 500 and 750 MHz. In (A) T_1 times at 500 MHZ, (B) T_2 times at 500 MHz, (C) T_1 times at 750 MHz; and (D) T_2 times at 750 MHz. Uncertainties are based on replicate experiments at given time points.

TABLE 3: Statistics on the Analysis of Diffusional Models for Cytochrome b_5

	χ^2	$\chi^{2\text{red}\ a}$	F[b]	$D_\parallel/D_\perp$[c]
isotropic	11232.35	158.2021		
axially symmetric	9238.066	135.8539	4.893	1.35 (1.17)
anisotropic	8809.659	133.4797	1.530	

[a] The reduced χ^2 is normalized to the number of degrees of freedom in the measurement. [b] For 72 measured values and one parameter in the fit versus three parameters in the fit for the axially symmetric case, the critical value for the *F*-statistic at a 95% confidence level is 3.14. [c] The ratio of $D_\parallel D_\perp$ for the axially symmetric diffusion model of motion for the oxidized protein. For comparison the observed $D_\parallel D_\perp$ for the reduced protein is included in parentheses. Uncertainties in this ratio are ± 0.01.

on the fit to the observed proton relaxation rate enhancements, contributions to the rates of ^{15}N relaxation can be calculated. The largest rate enhancements for ^{15}N nuclei are also contained in Table 2.

Figure 5 contains plots of the amplitudes of ^{15}N-relaxation parameters for the backbone amides of ferricytochrome b_5 at 500 and 750 MHz. Given the physical asymmetry of cytochrome b_5 evident in the solution structure of the protein, it is expected that a single rotational correlation time would be inadequate to describe global hydrodynamic properties. Using the R_2/R_1 ratio, an estimate of the effective global correlation time for a specific amide vector is obtained. Once these estimates have been obtained, it is possible to fit the behavior of the protein to a more realistic model of the reorientational motion using anisotropic diffusion tensor descriptions. Table 3 contains the statistics describing the improvement in fit quality for an axially symmetric diffusion tensor versus an isotropic model and a fully anisotropic model relative to the axially symmetric model. At a 95% confidence level, rat ferricytochrome b_5 is best described by an axially symmetric diffusion model. For comparison Table 3 also contains the ratio of parallel and perpendicular components of the axially symmetric

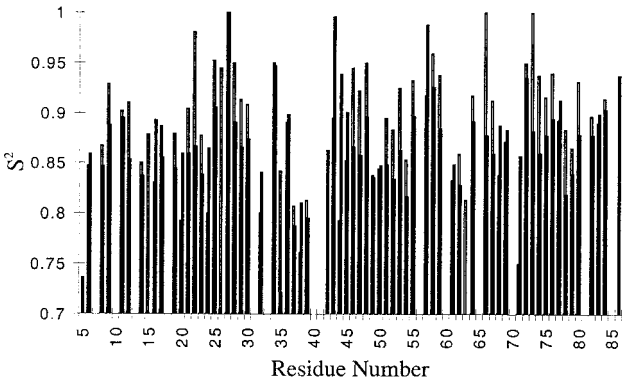

Figure 6. Comparison of the generalized order parameters determined for the reduced and oxidized forms of rat cytochrome b_5. Only the range from 0.7 to 1.0 is plotted in order to highlight differences in calculated order parameters. Black bars represent the oxidized protein and white outlined bars represent the reduced protein.

diffusion tensor determined for ferrocytochrome b_5. The magnitude of asymmetry observed for the oxidized cytochrome is slightly more than that observed for the reduced protein, perhaps consistent with the enhanced dynamic character of the oxidized protein described below.

Estimates of the local effective global correlation time for each of the amide vectors analyzed can also be obtained by optimizing the fit to the global correlation time for each residue using the program ModelFree 3.1. Estimates of the local effective global correlation time yielded in this manner are nearly identical to estimates obtained from the R_2/R_1 ratio. In addition, using this approach one can obtain a value for the generalized order parameter for each residue. A plot of generalized order parameters versus residue number is contained in Figure 6. Also contained in Figure 6 are the order parameters determined from the analysis of reduced cytochrome b_5. As can be seen from the plot, significant differences in the observed

order parameters are observed. The uncertainty in measured values based on replicate experiments is on the order of 3%.

The average value of the order parameter, S^2, for the oxidized rat cytochrome b_5 is 0.85. This differs significantly from recently reported values for the bovine protein[47] (i.e., $S^2_{av} = 0.8$). Differences between our measured values and those reported by Kelly et al.[47] may be attributable to a number of possible factors including differences in species variants, differences in hydrodynamic modeling of the cytochrome, or the inclusion of NOE values in the analysis.

Using eq 6 we can obtain an upper bound for the contribution of backbone dynamics to the observed entropy change. The contribution of conformational entropy obtained using eq 6 is generally assumed to be an upper bound because the assumption of uncorrelated motion of the amide bond vectors is clearly not correct for most proteins.[17] Recently, the applicability of eq 6 to systems of high rigidity (e.g., for amide vectors with S^2 values greater than 0.95) has been questioned[48] and it was suggested that care must be exercised in the application of calculations of conformational entropy based on classical approximations. Of the 68 residues examined in this study, nine have order parameters of 0.95 or greater. These residues which constitute 13% of the total, contribute 23% of the total entropy change. Thus, although the contribution of these residues is somewhat larger than the average contribution per residue, they do not dominate the total observed entropy change. It is important also to note that for two residues (e.g., residues 27 and 66) S^2 values equal to 1.0 were obtained from the model free analysis. Because eq 6 is not defined for S^2 values equal to unity, these residues were not included in the entropy analysis.

Given these caveats and using the results plotted in Figure 6 and contained in supplementary Table S-1, we obtain a value of 70 ± 6 J/K·mol. This result is remarkably similar to the total entropy change determined from the temperature dependence of the reduction potential described above (e.g., 60 ± 7 J/K·mol), which suggests that changes in backbone dynamics could play a significant role in determining the entropy change occurring on oxidation of cytochrome b_5.

Discussion

Theories Regarding the Dominant Effectors of Cytochrome Reduction Potentials. Many bioinorganic modeling[2,11] and mutagenic studies of cytochromes[5−10] have been performed in an attempt to understand the major protein−heme interactions which dictate reduction potentials. To date these studies have focused on energetic terms involving the modulation of iron orbital energy levels induced by changes in the local charge distribution about the heme,[5,8] the effect of reorientation of axial imidazoles[2,9,10] and the effect of changes in hydrogen bond strengths to the axial imidazoles.[11] Shifts in the reduction potentials of cytochrome *c* mutations are predicted with reasonable accuracy by using continuum models of the protein and solvent dielectric constants;[6] however, the magnitude of the changes observed in mutants of cytochrome *c*[7] are only on the order of 60 mV. Slightly larger shifts in reduction potentials are observed for mutants of cytochrome *c* peroxidase (e.g., slightly more than 100 mV for the D235E mutation[49]). Similar studies have been performed with cytochrome b_5, yielding shifts attributable to charge stabilization of the iron on the order of 20 mV.[8]

The effect of axial imidazole orientation has also been examined in detail. Theoretical estimates of the magnitude of this effect are on the order of 50 mV.[2] Mutational studies on cytochrome b_5 which have achieved a significant reorientation of the axial imidazole have resulted in shifts which are on the order of 20 mV.[9,10] The effects of changes in hydrogen bond strengths, which might be considered a subclass of local charge differences, have been evaluated based on bioinorganic modeling and amount to roughly 60 mV.[11] Thus, all energetic contributions to the differences in the electromotive driving force, based on mutational studies performed to date, are at most on the order of 100 mV. Yet there are examples, such as cytochrome b_{559}, within the photosynthetic apparatus of higher plants and cyanobacteria where the reduction potential can change from a low potential form of roughly 100 mV to a high potential form with a reduction of 400 mV with subtle as yet uncharacterized changes in the structure of the membrane bound protein complex.[3]

Contribution of Entropy to the Electromotive Driving Force. Here we suggest that entropic contributions to the electromotive driving force may play an equal or significantly greater role in modulating reduction potentials. The entropic contribution to the electromotive driving force in cytochrome b_5 at 298 K is 185 mV. If one considers the difference between cytochrome b_5 and the porphyrin model compound, a difference as large as 360 mV could be mediated by changes in entropy induced by changes in protein structure. This difference spans most of the accessible range of potentials of *b*-type cytochromes.

The heme cofactor is the most functionally diverse prosthetic group within the biosphere. Bioevolutionarily, the properties of this cofactor have been tuned to diametrically opposite roles. For example, the cytochromes have been evolutionarily bioengineered for facile electron transfer while proteins like myoglobin and hemoglobin have been designed evolutionarily to resist oxidation in a highly oxidative environment. The temperature dependence of the reduction potential of myoglobin is less well defined than that of the model porphyrin or cytochrome b_5 and thus the statistical significance of the calculated entropy change from the observed temperature variation is weak; however, it is interesting to note that the temperature dependence of myoglobin more closely resembles that of the model compound than that of the cytochrome, indicating that the entropy change is likely to be of opposite sign as indicated in Table 1. This is not due to solvent effects (at least not in the same manner as that observed in the model compound) in that the degree of solvent exposure and the orientation of the heme within myoglobin is strikingly similar to that of cytochrome b_5.

Studies of the backbone dynamics of cytochrome b_5 presented here have shown a striking similarity in the magnitude of entropic effects measured through an examination of the temperature dependence of the reduction potential and through differences observed in backbone dynamics. Clearly a variety of other system changes can contribute to the total entropy change and the total entropy change may involve the sum of several large terms of opposite sign. For example, the effects of side chain dynamics and changes in solvent exchange or the number of bound waters could significantly contribute to the total entropy change. Both of these contributions can be evaluated to a degree with NMR methods and such experiments are currently in progress. Nonetheless, we believe the correlation between the observed entropy change and the contribution of backbone dynamics indicates that redox coupled changes in hydrogen bond networks may be the primary event dictating observed changes in backbone dynamics and the entropy change of the system. Questions which remain to be answered are: What is the mechanism of coupling of the changes in the strength of hydrogen bond networks and the oxidation state of

the metal and what are the time scales involved in the changes in hydrogen bond strengths throughout the molecule?

Acknowledgment. This study made use of the National Magnetic Resonance Facility at Madison, which is supported by NIH Grant RR02301 from the Biomedical Research Technology Program, National Center for Research Resources. Equipment in the facility was purchased with funds from the University of Wisconsin, the NFS Biological Instrumentation Program (DMB-8415048), NSF Academic Research Instrumentation Program (BIR-9214394), NIH Biomedical Research Technology Program (RR02301), NIH Shared Instrumentation Program (RR02781 and RR08438), and the U.S. Department of Agriculture. The generous support of the National Institutes of Health (DK 46510, R. D. G.) and the National Science Foundation (CHE 9417357, C.J.M.) is gratefully acknowledged. Support from the NIH (S10RR10441) for the purchase of a 600-MHz NMR instrument housed in the UMAB NMR facility is also gratefully acknowledged.

Supporting Information Available: Table S-1 containing order parameters for both reduced and oxidized rat cytochrome b_5 calculated with the model free formalism (2 pages). See any current masthead page for ordering and Internet access instructions.

References and Notes

(1) Mathews, F. S. *Prog. Biophys. Mol. Biol.* **1985**, *45*, 1.
(2) Walker, F. A.; Huynh, B.-H.; Scheidt, W. R.; Osvath, S. R. *J. Am. Chem. Soc.* **1986**, *108*, 5288.
(3) Babcock, G. T.; Widger, W. R.; Cramer, W. A.; Oertling, W. A.; Metz, J. G. *Biochemistry* **1985**, *24*, 3638.
(4) Mathews, S.; Czerwinski, E. W.; Argos, P. In *The X-ray Crystallographic Structure of Calf Liver Cytochrome* b_5; Mathews, S., Czerwinski, E. W., Argos, P., Ed.; Academic Press: New York, 1979; Vol. VII, pp 107−147.
(5) Langen, R.; Brayer, G. D.; Berghuis, A. M.; McLendon, G.; Sherman, F.; Warshel, A. *J. Mol. Biol.* **1992**, *224*, 589.
(6) Zhou, H.-X. *J. Am. Chem. Soc.* **1994**, *116*, 10362.
(7) Cutler, R. L.; Davies, A. M.; Creighton, S.; Warshel, A.; Moore, G. R.; Smith, M.; Mauk, A. G. *Biochemistry* **1989**, *28*, 3188.
(8) Funk, W. D.; Lo, T. P.; Mauk, M. R.; Brayer, G. D.; MacGillivray-Ross, T. A.; Mauk, A. G. *Biochemistry* **1990**, *29*, 5500.
(9) Sarma, S.; Dangi, B.; Yan, C.-H.; DiGate, R. J.; Banville, D.; Guiles, R. D. *Biochemistry* **1997**, *36*, 5645.
(10) Sarma, S.; Banville, D.; DiGate, R. J.; Miller, C.; Guiles, R. D. *Biochemistry* **1997**, *36*, 5658.
(11) Quinn, R.; Mercer-Smith, J.; Burstyn, J. N.; Valentine, J. S. *J. Am. Chem. Soc.* **1984**, *106*, 4136.
(12) Terrettaz, S.; Cheng, J.; Miller, C.; Guiles, R. D. *J. Am. Chem. Soc.* **1996**, *118*, 7857.
(13) Cheng, J.; Terrettaz, S.; Blankman, J. I.; Miller, C. J.; Dangi, B.; Guiles, R. D. *Isr. J. Chem.* **1997**, *37*, 2.
(14) Palmer, A. G. *Curr. Opin. Biotechnol.* **1993**, *4*, 385.
(15) Dangi, B.; Sarma, S.; Yan, C.; Banville, D. L.; DiGate, R. J.; Guiles, R. D. *Biochemistry*, in press.
(16) Englander, J. J.; Englander, S. W.; Louie, G.; Roder, H.; Tran, T.; Wand, A. J. *Protein Hydrogen Exchange, Dynamics and Energetic*; Adenine Press: Guilderland, NY, 1988; Vol. 1, p 107.
(17) Akke, M.; Brüschweiler, R.; Palmer, A. G. I. *J. Am. Chem. Soc.* **1993**, *115*, 9832.
(18) Becka, A. M.; Miller, C. J. *J. Phys. Chem.* **1992**, *96*, 2657.
(19) Terrettaz, S.; Becka, A. M.; Traub, M. J.; Fettinger, J. C.; Miller, C. J. *J. Phys. Chem.* **1995**, *99*, 11216.
(20) Mori, S.; Abeygunawardana, C.; Johnson, M. O. N.; van Zijl, P. C. M. *J. Magn. Reson., Ser. B* **1995**, *108*, 94.
(21) Delaglio, F.; Grzesiek, S.; Vuister, G. W.; Zhu, G.; Pfeifer, J.; Bax, A. *J. Biomol. NMR* **1995**, *6*, 277.
(22) Tjandra, N.; Feller, S. E.; Pastor, R. W.; Bax, A. *J. Am. Chem. Soc.* **1995**, *117*, 12562.
(23) Brüschweiller, R.; Liao, X.; Wright, P. E. *Science* **1995**, *268*, 886.
(24) Banci, L.; Bertini, I.; Ferroni, F.; Rosato, A. *Eur. J. Biochem.* **1997**, *249*, 2270.
(25) Guiles, R. D.; Basus, V. J.; Sarma, S.; Malpure, S.; Fox, K. M.; Kuntz, I. D.; Waskell, L. *Biochemistry* **1993**, *32*, 8329.
(26) Sarma, S.; Banville, D.; DiGate, R. J.; Guiles, R. D. *J. Biomol. NMR* **1996**, *8*, 171.
(27) Guiles, R. D.; Basus, V. J.; Kuntz, I. D.; Waskell, L. *Biochemistry* **1992**, *31*, 11365.
(28) Palmer, A. G.; Williams, J.; McDermott, A. *J. Phys. Chem.* **1996**, *100*, 13293.
(29) Bertini, I.; Luchinat, C.; Vasavada, K. V. *J. Magn. Reson.* **1990**, *89*, 243.
(30) Vasavada, K. V.; Rao, B. D. N. *J. Magn. Reson.* **1989**, *81*, 275.
(31) Bertini, I.; Galas, O.; Luchinat, C.; Parigi, G. *J. Magn. Reson. Ser. A* **1995**, *113*, 151.
(32) Yamazaki, T.; Lee, W.; Arrowsmith, C. H.; Muhandiram, D. R.; Kay, L. E. *J. Am. Chem. Soc.* **1994**, *116*, 11655.
(33) Lipari, G.; Szabo, A. *J. Am. Chem. Soc.* **1982**, *104*, 4546.
(34) Lipari, G.; Szabo, A. *J. Am. Chem. Soc.* **1982**, *104*, 4559.
(35) Abragam, A. *The Principles of Nuclear Magnetism*; Clarendon Press: Oxford, 1961, pp 264−349.
(36) Mandel, A. M.; Akke, M.; Palmer, A. G. *J. Mol. Biol.* **1995**, *246*, 144.
(37) Tjandra, N.; Kuboniwa, H.; Ren, H.; Bax, A. *Eur. J. Biochem.* **1995**, *230*, 1014.
(38) Hoshino, M.; Ozawa, K.; Seki, H.; Ford, P. C. *J. Am. Chem. Soc.* **1993**, *115*, 9568.
(39) Blankman, J. I.; Miller, C. J.; Guiles, R. D. *J. Am. Chem. Soc.*, submitted for publication.
(40) Springer, B. A.; Sligar, S., G. *Proc. Natl. Acad. Sci.* **1987**, *84*, 8961.
(41) Marcus, R. A.; Sutin, N. *Biochim. Biophys. Acta* **1985**, *811*, 265.
(42) Rodgers, K. K.; Pochapsky, T. C.; Sligar, S. G. *Science* **1988**, *240*, 1657.
(43) Englander, S. W.; Sosnick, T. R.; Englander, J. J.; Mayne, L. *Curr. Opin. Struct. Biol.* **1996**, *6*, 18.
(44) Bertini, L.; Luchinat, C. *NMR of Paramagnetic Molecules in Biological Systems*; Benjamin/Cummings: Menlo Park, CA, 1986; p 77.
(45) Storch, E. M.; Daggett, V. *Biochemistry* **1995**, *34*, 9682.
(46) Veitch, N. C.; Whitford, D.; Williams, R. J. P. *FEBS Lett.* **1990**, *269*, 297.
(47) Kelly, G. P.; Muskett, F. W.; Whitford, D. *Eur. J. Biochem.* **1997**, 349.
(48) Yang, D.; Kay, L. E. *J. Mol. Biol.* **263**, 369.
(49) Goodin, D. B.; McRee, D. E. *Biochemistry* **1993**, *32*, 3313.